Catalysis Today 167 (2011) 77–83

Contents lists available at ScienceDirect

Catalysis Today

journal homepage: www.elsevier.com/locate/cattod

Mg–Zr mixed oxides for aqueous aldol condensation of furfural with acetone: Effect of preparation method and activation temperature

I. Sádaba [a], M. Ojeda [a], R. Mariscal [a], R. Richards [b], M. López Granados [a,*]

[a] Institute of Catalysis and Petrochemistry (CSIC), C/Marie Curie, 2, 28049 Madrid, Spain
[b] Department of Chemistry and Geochemistry, Colorado School of Mines, Golden, CO 80401, USA

ARTICLE INFO

Article history:
Received 20 May 2010
Received in revised form 8 October 2010
Accepted 2 November 2010
Available online 21 December 2010

Keywords:
Co-precipitation
Alcogel
Claisen–Schmidt condensation
Biofuels

ABSTRACT

Mg–Zr (Mg/(Mg + Zr) = 0.5, nominal atomic ratio) catalysts have been synthesized following two different preparation methods (co-precipitation and alcogel) and tested in furfural/acetone aldol condensation reactions. The untreated co-precipitated solid shows the presence of $Mg(OH)_2$ and Zr oxyhydroxide-like phases, which are not very active in the furfural/acetone aldol condensation. When the solid is treated in O_2/Ar flow at increasing temperatures (up to 873 K), the initial phases evolve to a mixture of cubic $Mg_xZr_{1-x}O_{2-x}$ mixed oxide and MgO. The latter phase (cubic MgO) shows a significantly enhanced catalytic activity. In contrast, the same species are already generated in the solid obtained in the alcogel route. Nevertheless, this latter preparation method also requires a high temperature treatment step to form highly active catalysts in furfural/acetone aldol condensation because the ethoxy residues originated during aerogel preparation need to be removed.

1. Introduction

The biorefinery system is based on biomass as processing input (feedstock) for the production of a multiple variety of bio-based products and fuels via a combination of physical and chemical processes. A critical requisite to assure the sustainability of these biorefineries is the availability and utilization of large amounts of currently under utilized resources, such as different residues (agricultural, forest, municipal and industrial) and/or non-edible crops [1]. Since the chemical composition of these materials consists primarily of lignocellulose, the development of appropriate technologies to convert the cellulose, hemicellulose and lignin components into biofuels and bioproducts will be essential for the successful establishment of future biorefineries.

Furfural, obtained predominantly from biomass-derived C_5 carbohydrates [2], possesses great potential as a key compound in the valorization of the hemicellulose contained in biomass when considering the development of a modern biorefinery concept. Thus, furfural can be transformed into a variety of important industrial chemicals by hydrogenation, oxidation, reductive amination, decarbonylation, nitration, condensations, etc. [2,3]. This latter valorization route of furfural, in particular, aqueous aldol condensation with acetone, has been recently proposed by Dumesic and co-workers as an intermediate step for the synthesis of second generation biofuels from monosaccharides obtained from lignocellulosic biomass [4]. In this process, biomass-derived furfural reacts with acetone to form molecules with a specific number of carbon atoms (C_8 and C_{13}) that can be further processed via successive hydrogenation and dehydration steps to form the corresponding pool of linear C_8–C_{13} alkanes [5]. Aldol condensation reactions of furfural are also of interest to form furfurylidene ketone-based compounds, which may have applications as aromas in the food industry [6] and as monomers for furan derived resins [7]. The aldol condensation reaction is typically performed in an organic solvent via homogeneous catalysis, usually by adding NaOH [6,8]. However, the aldol condensation reactions should be carried out ideally in aqueous media because the development of green and sustainable catalytic processes in biorefineries requires the use of non-toxic and inexpensive solvents. Moreover, furfural is currently obtained in industry as aqueous solutions, and therefore, performing the aldol condensation in water would avoid costly furfural/solvent separation steps by distillation. In addition, the use of solid materials (instead of homogeneous catalysts) is preferred in order to avoid expensive separation processes downstream and to decrease the negative environmental impact. Therefore, it is of great interest to find water tolerant solid catalysts to accomplish the furfural/acetone aldol condensation reaction. Okuhara has recently published an extensive review about water-tolerant acid catalysts [9]. In contrast, the use of solid base catalysts in water is poorly understood. MgO has been widely used in base-catalyzed chemical reactions in gas phase, although its use in water affects

* Corresponding author at: Institute of Catalysis and Petrochemistry (CSIC), C/Marie Curie, 2, 28049 Madrid, Spain. Tel.: +34 915854937; fax: +34 91 5854760.
E-mail address: mlgranados@icp.csic.es (M.L. Granados).

0920-5861/$ – see front matter © 2010 Elsevier B.V. All rights reserved.
doi:10.1016/j.cattod.2010.11.059

the pH value [10] and leads to the formation of the corresponding hydroxide [11,12], which may display a different catalytic behavior.

Here, we report on the utilization of Mg–Zr mixed oxides as catalysts in the aldol condensation reaction of furfural and acetone in aqueous media. We have added zirconium species during the preparation of the MgO-based solids in an attempt to improve their stability in water. Dumesic and co-workers have already reported the successful use of this type of materials in furfural/acetone aldol condensation [4,13]. Nevertheless, additional investigations are required with the aim of improving the catalytic yields and understanding structure–activity relationships. In particular, we have focused on the effects of the preparation method (co-precipitation and alcogel) and activation temperature on the activity and selectivity values shown in the aqueous furfural/acetone aldol condensation. This work complements our parallel study showing that a co-precipitated MgZr sample with a Mg/(Mg + Zr) atomic ratio equals to 0.5 presents the highest intrinsic activity values [14]. Here, we extend these previous studies with novel preparation techniques (alcogel methodology).

2. Experimental

2.1. Catalysts preparation

Catalysts were synthesized following two different preparation methods: co-precipitation (CO) and alcogel (AL). In the co-precipitation method, $Mg(NO_3)_2{\cdot}6H_2O$ (16.0 g, Sigma–Aldrich, >98%) and $ZrO(NO_3)_2{\cdot}xH_2O$ (22.0 g, Alfa Aesar, 99.9% metal) were dissolved in deionized water (1 L), as previously reported by Aramendia et al. [15]. The x value for the $ZrO(NO_3)_2{\cdot}xH_2O$ was determined to be 6 by thermogravimetric analysis. The mixture (Mg/(Mg + Zr) = 0.5, nominal atomic ratio) was stirred (500 rpm) at room temperature and a NaOH solution (25 wt.%, Sigma–Aldrich, >98%) was added at constant rate (*ca.* 1 cm^3 min^{-1}) until pH = 10. The precipitate was aged under these conditions for 72 h. The solid was subsequently recovered by filtration under vacuum and washed with 5–10 L of deionized water until constant conductivity. Finally, the solid was treated in ambient air at 383 K for 24 h and then stored in N_2.

According to the alcogel preparation method previously described by Chen et al. [16], $Mg(NO_3)_2{\cdot}6H_2O$ (3.9 g, Sigma–Aldrich, >98%) and $ZrO(NO_3)_2{\cdot}xH_2O$ (5.1 g, Sigma–Aldrich, 99%) were dispersed in ethanol (100 cm^3, Pharmco-Aaper). The mixture was then heated to 383 K for 1 h in an autoclave, which leads to the formation of the corresponding alcogel. The solid was then cooled down and kept at room temperature for 1 h. Afterwards, ethanol (200 cm^3) was added and He (1.0 MPa) was introduced in the autoclave to perform supercritical fluid drying at 538 K for 4 h. Next, the pseudo-supercritical solution was vented to release the pressure and then cooled down in He.

The precursors (denoted as -*p*) obtained in the co-precipitation and alcogel methods (named as CO and AL, respectively) were submitted to thermal treatment in O_2/Ar flow (25 vol.%) from room temperature to 573 K (denoted as -LT, low temperature) or 873 K (denoted as -HT, high temperature) at 5 K min^{-1} and keeping at the corresponding temperature for 1 h. As explained later, selection of treatment temperatures is based on characterization data (Section 3.2).

2.2. Measurements of catalytic activity

Furfural (1.3 cm^3, 15.7 mmol, Fluka, >99.0%) and deionized water (40 cm^3) were mixed in a discontinuous batch-type glass reactor (100 cm^3). Ambient air was previously removed by flushing with N_2 (100 cm^3 min^{-1}) for 1 h. The temperature of the furfural-water mixture was then increased under stirring (800 rpm) to the desired value (333 K). Subsequently, the powder catalyst (0.1 g) and acetone (10 cm^3, 136.4 mmol, Riedel-de-Häen, 99.8%) were added to initiate the catalytic reaction. The catalysts were activated in an ex situ reactor by flowing 25 vol.% O_2/Ar (50 cm^3 min^{-1}) and, once at room temperature, directly poured in the flushed reactor to prevent the carbonation and the hydration by contact with ambient air. The aliquots were periodically withdrawn from the reaction mixture with a syringe and then filtered with a Captiva™ (Varian Inc., 450 nm pore diameter) column. The filtered aqueous solution contains the unreacted furfural and acetone, as well as a fraction of the reaction products. The water-insoluble fraction of the reaction products was retained in the column filter and dissolved by passing tetrahydrofurane (Riedel-de-Häen, 99.9%) through the column. An organic phase containing the water-insoluble reaction products was then collected. A determined amount of *n*-butanol (Fluka, 99.5%) was added to both the aqueous and organic phase as an internal standard for the quantitative analysis with a gas chromatograph (Varian CP-3800) equipped with a flame ionization detector (FID) and a HP-5 capillary column (30 m × 0.32 mm). Further details of the analysis are given in the Supplementary Information section and elsewhere [14].

2.3. Characterization techniques

Thermogravimetric analyses (TGA) were performed with a Mettler Toledo TGA/SDTA 851e equipment upon treating the samples in N_2 atmosphere from room temperature to 1373 K at a heating rate of 10 K min^{-1}.

Elemental chemical composition was determined with an inductively coupled plasma mass spectrometer (ICP-MS) Elan 6000 Perkin-Elmer Sciex equipped with an autosampler AS 91. The different samples were previously digested in a high-pressure microwave oven (Milestone ETHOS PLUS) with an aqueous solution of HCl and HNO_3.

Powder X-ray diffraction (XRD) patterns were recorded in the 15–80° 2θ range in scan mode (0.02°, 1 s) using an X'Pert Pro PANalytical diffractometer with Cu Kα_1 (λ = 0.154046 nm) and Cu Kα_2 (λ = 0.154443 nm) radiations (Kα_1/Kα_2 = 0.5). Diffractograms were analyzed with the X'Pert HighScore Plus software.

N_2 adsorption–desorption isotherms were recorded at the temperature of liquid nitrogen (77 K) using a Micromeritics TRISTAR 3000 apparatus. Samples were degassed at 393 K for 12 h prior to the determination of the adsorption isotherm. Surface area values were calculated using the Brunauer–Emmett–Teller (B–E–T) equation.

X-ray photoelectron spectroscopy (XPS) experiments were accomplished with a VG Escalab 200 R Fisons spectrometer equipped with Al Kα ($h\nu$ = 1486.6 eV) and Mg Kα ($h\nu$ = 1253.6 eV) X-ray sources. Kinetic energies of photoelectrons were measured by using a hemispherical electron analyzer working in the constant pass energy mode. The background pressure in the analysis chamber was kept below 5×10^{-8} mbar during data acquisition. The powder samples were previously treated in O_2/Ar at the given temperature as indicated above and once activated, the samples were immediately poured into a flask containing isooctane. The soaking in isooctane prevent the contact with ambient during the subsequent handling. Then, the solids were rapidly pressed into copper holders, mounted on a support rod placed in the pretreatment chamber to remove the protecting agent (isooctane). Binding energies were calibrated relative to the C 1s peak from carbon contamination of the samples at 284.6 eV to correct the contact potential differences between the sample and the spectrometer. Both binding energy values and peak areas were computed by fit-

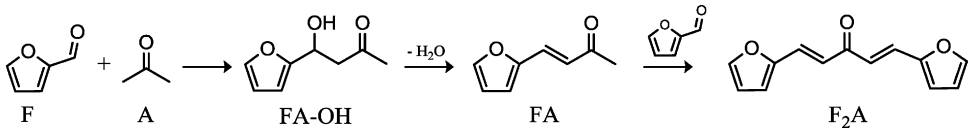

Scheme 1. Reactions involved in the base-catalyzed aldol condensation of furfural with acetone.

ting the experimental spectra to Gaussian/Lorentzian lines after removal of a S-shaped background. Surface atomic ratios were calculated from peak area ratios normalized by atomic sensitivity factors [17].

3. Results and discussion

3.1. Catalytic activity

Scheme 1 shows the set of consecutive reactions that form the main products of the aqueous base-catalyzed aldol condensation of furfural (F) with acetone (A).

The abstraction of an α-H atom of acetone by the base catalyst forms an intermediate carbanion species, which reacts subsequently with the carbonyl group of furfural to form a C_8 monomer, 4-(2-furanyl)-4-hydroxybutan-2-one (named as FA-OH hereafter). This species undergoes dehydration to form an α,β-unsaturated ketone, 4-(2-furanyl)-3-buten-2-one or furfurylidene acetone (FA). A second condensation reaction of FA with another furfural molecule yields the dehydrated C_{13} aldol-adduct dimer, 1,5-bis-(2-furanyl)-1,4-pentadien-3-one or difurfurylidene acetone (F_2A). All these products have been detected in the aqueous condensation of furfural with acetone [8,18–20]. Both FA and F_2A molecules can polymerize leading to black cross-linked heavier materials [8,18,19]. The condensation reaction between two acetone molecules is chemically feasible, but the rate is significantly lower when compared to that of furfural-acetone condensation. Self aldol-condensation between two furfural molecules is not possible because of the absence of hydrogen atoms in the α position with respect to the carbonyl group.

The formation of FA-OH, FA and F_2A accounts for 95–100% of the reaction products (carbon balance) obtained at 333 K with the MgZr solids prepared by either co-precipitation or alcogel for conversions up to 50–60%. Therefore, we compare the activity displayed by the different catalysts by means of the overall yield values calculated from the products detected in the gas chromatograph (Fig. 1).

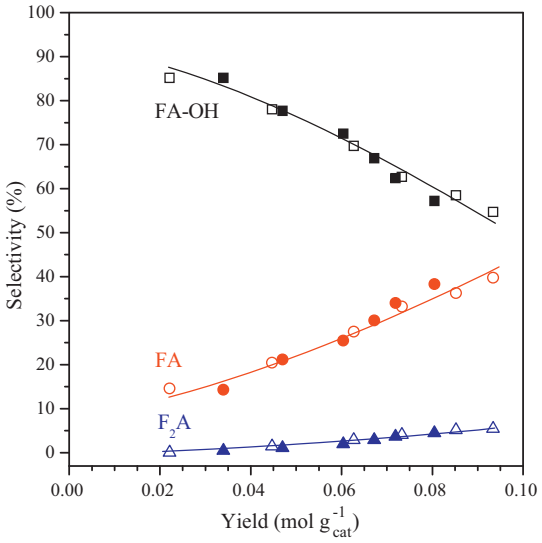

Fig. 2. Selectivity values obtained in furfural/acetone aldol condensation (333 K, 0.1 g catalyst, 1.3 cm^3 furfural, 10 cm^3 acetone, 40 cm^3 water). Open and closed symbols correspond to MgZr-CO-HT and MgZr-AL-HT catalysts, respectively.

First, we note that irrespective of the preparation method used to synthesize the MgZr materials, these need to be treated at elevated temperature (873 K) in order to obtain high yields to the reaction products. The catalytic activity values shown by these materials are very similar. Furthermore, we find that regardless of the synthesis route, the catalytic activity of the untreated and low-temperature treated solids is almost undistinguishable.

Selectivity values to the three main reaction products (FA-OH, FA and F_2A) obtained with the most active samples (MgZr-CO-HT and MgZr-AL-HT) at different furfural conversion levels are depicted in Fig. 2. Products distribution is identical with both samples, indicative of common kinetically-relevant steps in the

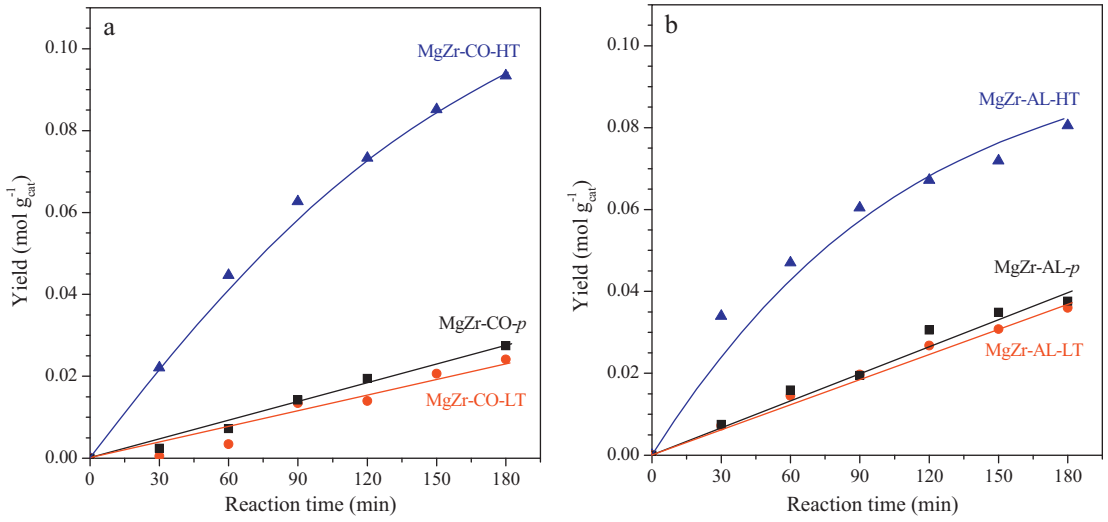

Fig. 1. Yield to reaction products obtained in furfural/acetone aldol condensation (333 K, 0.1 g catalyst, 1.3 cm^3 furfural, 10 cm^3 acetone, 40 cm^3 water) with MgZr solids prepared by co-precipitation (a) or alcogel (b).

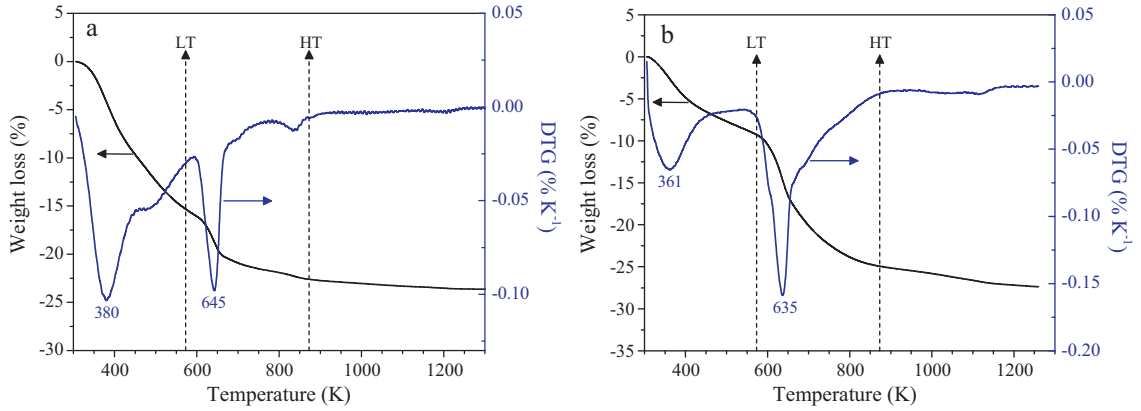

Fig. 3. Thermal profiles of the MgZr precursor prepared via co-precipitation (a) or alcogel (b).

sequence shown in Scheme 1. We note also that the hydrated monomer (FA-OH) is predominantly formed over dehydrated monomer (FA) and dimer (F_2A) at all furfural conversion levels. Selectivity to FA-OH decreases with increasing furfural conversion, while the opposite trend is found for FA selectivity. Minor amounts (<5%) of F_2A are detected at all conversion values, probably because of the high acetone/furfural molar ratios used (A/F *ca.*10) [8].

3.2. Catalysts characterization

The thermal evolution of the precursors prepared by co-precipitation and alcogel was investigated by thermogravimetric analysis (TGA and DTG; Fig. 3). The MgZr precursor prepared by co-precipitation displays two significant weight reduction processes centered at 380 and 645 K in the thermal profiles (Fig. 3a), which would correspond, respectively, to the dehydration of Zr hydroxide and Mg hydroxide species (evidenced by evolved gas analysis by mass spectrometry; results not shown) [15]. We have noticed that the measured overall diminution of weight is lower than that it would correspond to the stoichiometric dehydration precursors to give ZrO_2 and MgO, respectively. This strongly suggests the presence of other species, as zirconium oxyhydroxide species, $ZrO_2(H_2O)_x$, as already found by other authors and commonly referred as hydrous zirconia [21,22]. The TGA/DTG profiles obtained with the solid prepared via alcogel are shown in Fig. 3b. We observe two weight loss processes at 361 and 635 K, which, in principle, could be assigned to the dehydration of precursors, as already described for the co-precipitated sample. However, X-ray diffraction (shown later) reveals that a cubic Mg–Zr mixed oxide phase (c-$Mg_xZr_{1-x}O_{2-x}$) instead of oxyhydroxide is already formed in the alcogel route. Therefore, the assignment of the two weight losses observed in the TGA profile is different in this latter case. Thus, we attribute the first peak (361 K) to the desorption of physically adsorbed water, while the second weight loss process (635 K) corresponds to the thermal decomposition of nitrate and ethoxy groups remaining in the sample [16]. The latter results were confirmed by evolved gas analysis by mass spectrometry: H_2O was observed for the first peak, while H_2O, CO, CO_2 (ethoxy decomposition by combustion) and minor amounts of NO_2 (nitrate decomposition) were detected in the second process. Nitrogen oxides detection is consistent with the magnesium nitrate hydroxide found in this precursor (see XRD results below).

Based on the analysis of the TGA/DTG profiles obtained with the MgZr samples prepared via co-precipitation and alcogel, these solids were treated at low and high temperatures (573 and 873 K, respectively; shown in Fig. 3). Nomenclature and calculated specific surface areas from N_2 adsorption-desorption isotherms at 77 K are listed in Table 1. Surface area values of the samples prepared via alcogel are significantly higher (1.7–1.9 times) than those of their respective co-precipitated counterparts. In both cases, increasing the treatment temperature yields solids with reduced surface areas.

Chemical analysis by ICP-MS of the MgZr solids prepared by co-precipitation or alcogel methodology and treated at low and high temperature reveals that the amount of Mg incorporated into the solids (expressed as the Mg/(Mg + Zr) atomic ratio) is slightly inferior to the nominal value (close to 0.40 for co-precipitation and alcogel *versus* 0.50). This may reflect an hydration value for $Mg(NO_3)_2{\cdot}6H_2O$ larger than that provided for the chemical supplier ($x = 6$). We also speculate that, in the case of the co-precipitated solids, the incomplete precipitation of Mg^{2+} species as $Mg(OH)_2$ may occur at the conditions used here (298 K and pH = 10). Another explanation, also valid for the -CO samples, is that the magnesium hydroxide species formed during co-precipitation were partially removed during the washing steps with water. Indeed, we found that as the number of washing steps increased, the conductivity of the rinsing water decreased until reaching a constant value slightly above that of deionized water.

X-ray diffraction patterns obtained with the untreated (denoted here as -p) and the thermally treated (at low or high temperature) precursors are depicted in Fig. 4. Crystalline hexagonal $Mg(OH)_2$ (Inorganic Crystal Structure Database (ICSD) #034401) is exclusively observed for the co-precipitated MgZr precursor (MgZr-CO-p; Fig. 4a). We also consider the presence of an XRD-undetectable amorphous zirconium oxyhydroxide, as TGA/DTG

Table 1
Nomenclature, surface area and crystallite size of the phased detected in the MgZr solids prepared by co-precipitation or alcogel methodology.

Nomenclature	Preparation	Treatment (K)	S_{BET} ($m^2\ g^{-1}$)[a]	Crystallite size (nm)[b]		
				$Mg_xZr_{1-x}O_{2-x}$	$Mg(OH)_2$	MgO
MgZr-CO-LT	Co-precipitation	573	184	–	24.9	–
MgZr-CO-HT	Co-precipitation	873	114	17.4	–	10.2
MgZr-AL-LT	Alcogel	573	311	4.7	–	8.8
MgZr-AL-HT	Alcogel	873	215	3.4	–	14.4

[a] Specific surface area measured according to the Brunauer–Emmett–Teller theory.
[b] Determined by XRD patterns. The following reflections at 2Θ were used: 30.5° for $Mg_xZr_{1-x}O_{2-x}$, 38° for $Mg(OH)_2$ and 42.9° for MgO.

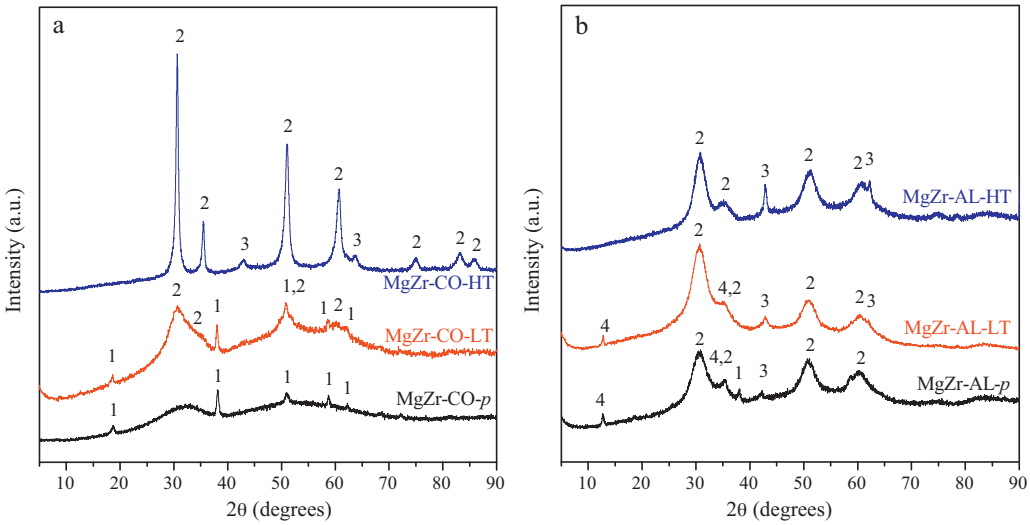

Fig. 4. X-ray diffraction patterns of the solids prepared via co-precipitation (a) or alcogel (b). Phases identification: hexagonal $Mg(OH)_2$ (1); cubic $MgZrO_x$ mixed oxide (2); cubic MgO (3); hexagonal $Mg_2(OH)_{3.24}(NO_3)_{0.76}(H_2O)_{0.24}$ (4).

evidenced the dehydration of this phase. When the co-precipitated precursor is treated in O_2/Ar flow at relatively low temperature (573 K; MgZr-CO-LT), we detect the same crystalline $Mg(OH)_2$ species as well as the incipient appearance of new poor-crystallized phases, cubic Mg–Zr mixed oxide (*c*-$Mg_xZr_{1-x}O_{2-x}$, ICSD #060443). At higher calcination temperatures (873 K; MgZr-CO-HT), *c*-$Mg_xZr_{1-x}O_{2-x}$ mixed oxide becomes better crystallized and cubic MgO (ICSD #060692) is formed by dehydration of $Mg(OH)_2$. We have previously determined that the mixed oxide is formed when Mg^{2+} ions are incorporated into a cubic ZrO_2 structure [14]. The identification of the $Mg_xZr_{1-x}O_{2-x}$ mixed oxide as a cubic or tetragonal phase is not straightforward by XRD because of the similarity of the corresponding diffraction patterns. Nevertheless, Castro et al. [23] have unequivocally determined by Raman spectroscopy that a cubic structure for the *c*-$Mg_xZr_{1-x}O_{2-x}$ mixed oxide is predominantly stabilized in ZrO_2 nanopowders containing MgO as additive at the atomic Mg/(Mg + Zr) = 0.5. Furthermore, other authors have reported that cubic zirconia is predominantly formed when doping with lower valence ions, as it is indeed the case of Mg^{2+} [24].

Interestingly, the identity of the phases initially formed following the alcogel protocol and their evolution with the treatment temperature are significantly different (Fig. 4b). In this case, we observe that the crystalline *c*-$Mg_xZr_{1-x}O_{2-x}$ mixed oxide phase is already present in the untreated precursor (MgZr-AL-*p*), probably as a result of the supercritical drying step at 538 K during the preparation method. Besides, diffraction lines attributed to MgO, $Mg(OH)_2$ and magnesium nitrate hydroxide hydrate ($Mg_2(OH)_{3.24}(NO_3)_{0.76}(H_2O)_{0.24}$) (PDF reference code 00-047-0436) also appear in the precursor. As the solid is treated at 573 and 873 K (MgZr-AL-LT and MgZr-AL-HT, respectively), the *c*-$Mg_xZr_{1-x}O_{2-x}$ mixed oxide is better crystallized as deduced by the narrowing of the diffraction data, while the magnesium hydroxide and nitrate hydroxide are progressively transformed into cubic MgO.

Summarizing the XRD results, we find that the same crystalline phases are detected after treating at 873 K the solids prepared by co-precipitation and alcogel: cubic $Mg_xZr_{1-x}O_{2-x}$ mixed oxide and cubic MgO. However, differences are evident for the solids treated al low temperature (573 K). Thus, $Mg(OH)_2$ is exclusively observed for the co-precipitated solid, while *c*-$Mg_xZr_{1-x}O_{2-x}$ and MgO are already formed in the alcogel route.

Table 1 shows the crystallite sizes calculated from the Scherrer equation for the phases formed after treating the solids at 573 or 873 K. We observe that the alcogel preparation method leads to significantly smaller *c*-$Mg_xZr_{1-x}O_{2-x}$ mixed oxide crystallites (3.4 nm *versus* 17.4 nm for the alcogel and co-precipitation methods, respectively). In contrast, unimportant differences in MgO crystallites sizes are found with the solids prepared following the alcogel or co-precipitation protocol (14.4 nm *versus* 10.2 nm for the alcogel and co-precipitation methods, respectively). Moreover, we note that the size of the *c*-$Mg_xZr_{1-x}O_{2-x}$ mixed oxide crystallites in the alcogel sample remain mostly unaffected by the treatment temperature, while those of MgO agglomerate as this temperature is increased.

Table 2 shows a summary of the most relevant X-ray photoelectron spectroscopy (XPS) results obtained for the Mg 2s, O 1s, Zr 3d, and C 1s core levels. The binding energy of the Mg 2s core level appears at 88.0-89.1 eV for all samples, corresponding to Mg^{2+} species. The component Zr $3d_{5/2}$ is observed at 181.4–181.8 eV, and it is ascribed to Zr^{4+} species in ZrO_2. The O 1s core level must have a complex composition as O^{2-} from MgO, ZrO_2, and *c*-$Mg_xZr_{1-x}O_{2-x}$ mixed oxide, as well as oxygen atoms in different hydroxyl groups

Table 2
Summary of the most relevant XPS features of the MgZr solids.

Sample	Binding energy (eV)				Mg/Zr atomic ratio	
	Mg 2s	O 1s	Zr $3d_{5/2}$	C 1s	XPS	ICP-MS
MgZr-CO-LT	88.0	530.7	181.4	284.5 289.3	1.8	0.7
MgZr-CO-HT	89.1	530.3	181.8	284.5	2.7	0.7
MgZr-AL-LT	88.1	530.2	181.4	284.6 288.1	0.5	0.6
MgZr-AL-HT	88.4	530.1	181.6	284.6	2.9	0.6

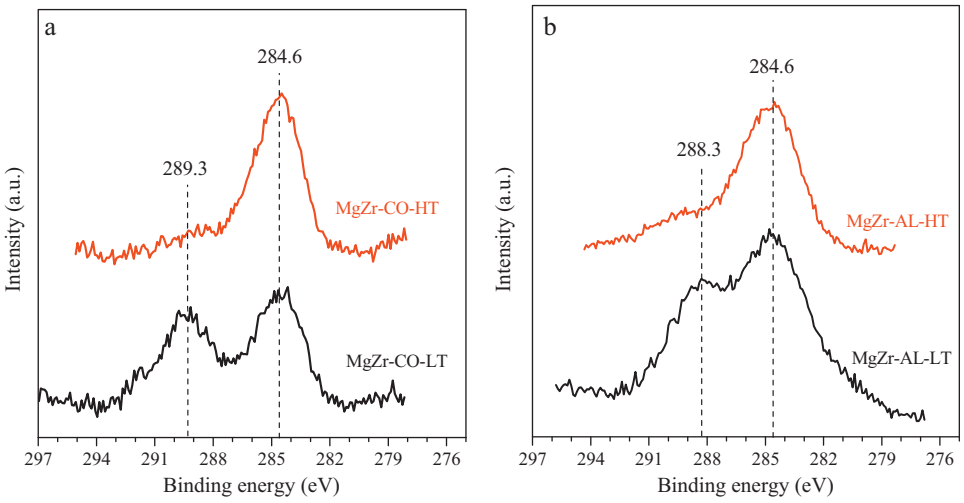

Fig. 5. X-ray photoelectron spectra (C 1s region) of MgZr solids prepared via co-precipitation (a) or alcogel (b).

can contribute to the overall O 1s peak. Actually, the O 1s core level displays an important asymmetry (results not shown) denoting a complex nature. Finally, the C 1s peak at *ca.* 284.6 eV corresponds to adventitious hydrocarbon contamination from ambient air. However, an additional C 1s component is noticed in the solids treated at low temperature (Fig. 5). Thus, the sample MgZr-CO-LT shows a XPS feature at 289.3 eV as a result of the carbonatation phenomenon that may occur during co-precipitation and drying of the precursor under ambient air. We note that these carbonates species are removed when the solid is treated at high temperature (Fig. 5a). The sample MgZr-AL-LT also displays an additional C 1s peak at 288.3 eV (Fig. 5b), although in this case, this component can be assigned to C-O in organic species that reflects the presence of ethoxy groups on the catalyst surface. Consistent with the TGA profiles, XPS also shows that these latter species are removed when treating the solid at high temperature.

The surface Mg/Zr atomic ratio measured by XPS with the sample prepared by co-precipitation (1.8 for MgZr-CO-LT) is higher than that obtained for the bulk material by ICP-MS (0.7), which may evidence the preferential location of Mg-containing species on the solid surface [23]. Moreover, the Mg/Zr atomic ratio increases up to 2.7 with the temperature treatment at high temperature, reflecting the segregation of MgO species. The higher Mg/Zr ratio in the AL-HT may reveal a remarkable sintering of the *c*-$Mg_xZr_{1-x}O_{2-x}$ mixed oxide (as evidenced by the narrower XRD lines) sample that would result in the lowering of the intensity of the XPS surface Zr signal and the concomitant increased in the Mg/Zr atomic ratio.

Interestingly, the surface Mg/Zr atomic ratio measured by XPS for MgZr-AL-LT is relatively similar to that obtained for the bulk solid (0.5 and 0.6, respectively), indicating that the *c*-$Mg_xZr_{1-x}O_{2-x}$ mixed oxide is more resistant against sintering and/or MgO segregation at this temperature. In addition, the relatively low Mg/Zr atomic ratio could be in part explained by the preferential bonding of the ethoxy groups over the Mg atoms. Nevertheless, the surface Mg/Zr atomic ratio for MgZr-AL-HT increases significantly as a result of the segregation of the Mg species and/or removal of the ethoxy groups, as it also occurs for the co-precipitated sample.

In summary, although the alcogel methodology provides a very intimate mixture of both Mg^{2+} and Zr^{4+} ions (formation of the *c*-$Mg_xZr_{1-x}O_{2-x}$ mixed oxide in the as-prepared solid), segregation of phases probably occurs during the thermal treatment in the same direction as in the co-precipitated sample. Eventually, the Mg/Zr atomic ratio for the samples treated at 873 K is almost identical, irrespective of the preparation method used.

3.3. Structure–activity relationships

According to our XRD data, the co-precipitated samples MgZr-CO-*p* and MgZr-CO-LT display only diffraction lines attributed to $Mg(OH)_2$ and an incipient *c*-$Mg_xZr_{1-x}O_{2-x}$ mixed oxide in the latter solid. Amorphous Zr oxyhydroxide is also present, as deduced by TGA/DTG analyses. All these species are not very active in the furfural/acetone aldol condensation reaction. When this solid is calcined at high temperature, the activity increases and MgO and *c*-$Mg_xZr_{1-x}O_{2-x}$ mixed oxide are formed. Since the *c*-$Mg_xZr_{1-x}O_{2-x}$ mixed oxide is already present in the LT sample, it seems very reasonable to assume that the larger activity found for MgZr-CO-HT can be associated to certain surface sites present in the MgO phase. The catalytic behavior of the -AL samples can be also explained by assuming that the MgO is associated with the highest activity. Thus, as demonstrated by XRD and TG/DTA studies, calcination at higher temperatures is required to fully decompose the MgO precursor and to remove the organic residues from both the bulk and the surface. It is very likely that the strong basic sites associated to surface Mg–O centers are involved in the reaction mechanism.

On the other hand, when the used catalyst was utilized for a second run, their activity was significantly smaller than that of the fresh catalysts. One of the possible causes of deactivation is the formation of $Mg(OH)_2$ by hydration of MgO, while the $Mg_xZr_{1-x}O_{2-x}$ phase remains unaltered [14]. When the used catalysts are re-calcined at 873 K and the Mg hydroxide is transformed again into MgO, the catalyst largely recovered its activity, indicating that the most active sites are associated to MgO.

Additional support to our hypothesis that $Mg_xZr_{1-x}O_{2-x}$ phase is less active and that activity is largely associated to MgO is also derived from the fact that the crystal size of the $Mg_xZr_{1-x}O_{2-x}$ phase in MgZr-AL-HT sample is smaller than that in MgZr-CO-HT. Therefore, the former must exhibit a larger number of surface sites than the MgZr-CO-HT sample, and consequently, a larger activity. In contrast, the activity of both samples is, however, similar, indicting therefore that the contribution of this phase to the overall activity must be less important than that associated to MgO.

4. Conclusions

Clear differences in the chemical, textural and structural properties are found for the MgZr precursors prepared via co-precipitation and alcogel routes and in the catalysts derived from them by calcination. However, these differences appear to be non-influential for the catalytic properties. Calcination at 873 K is required for both

precursors to deploy the largest activity. In the case of the co-precipitated route, the most active phase, MgO, is only formed by calcination at 873 K. In the alcogel precursor, the MgO is formed by calcination at lower temperature (573 K) but calcinations at 873 K is required to remove the ethoxy residues left over the surface because of the alcogel methodology. The intrinsic activity of c-$Mg_xZr_{1-x}O_{2-x}$ mixed oxide is smaller than that of MgO, and its contribution to the overall conversion is consequently smaller.

Acknowledgements

The Spanish Ministry of Science and Innovation (MICINN) and "Consejería de Educación" of the Autonomous Government of Madrid (CAM) is grateful acknowledged for financial support through the projects ENE-2009-12743-C04-01 and CARDENER-CM, respectively. I. Sádaba and M. Ojeda thank the Spanish National Research Council (CSIC) for their contracts under the program JAE-Predoc and JAE-Doc, respectively. R. Richards thanks the Colorado School of Mines for financial support.

Appendix A. Supplementary data

Supplementary data associated with this article can be found, in the online version, at doi:10.1016/j.cattod.2010.11.059.

References

[1] S.N. Naik, V.V. Goud, P.K. Rout, A.K. Dalai, Renew. Sustain. Energy Rev. 14 (2010) 578.
[2] K.J. Zeitsch, The Chemistry and Technology of Furfural and its Many By-products, Elsevier Science, Amsterdam, 2000.
[3] A. Corma, S. Iborra, A. Velty, Chem. Rev. 107 (2007) 2411.
[4] G.W. Huber, J.N. Chheda, C.J. Barrett, J.A. Dumesic, Science 308 (2005) 1446.
[5] R.M. West, Z.Y. Liu, M. Peter, C.A. Gärtner, J.A. Dumesic, J. Mol. Catal. A: Chem. 296 (2008) 18.
[6] N. Fakhfakh, P. Cognet, M. Cabassud, Y. Lucchese, M. Días de Los Ríos, Chem. Eng. Process. 47 (2008) 349.
[7] A. Gandini, M.N. Belgacem, Prog. Polym. Sci. 22 (1997) 1203.
[8] D.A. Isacescu, I. Gavat, C. Stoicescu, C. Vass, I. Petrus, Rev. Roum. Chim. 10 (1964) 219.
[9] T. Okuhara, Chem. Rev. 102 (2002) 3641.
[10] K. He, Y.M. Dong, Z. Li, L. Yin, A.M. Zhang, Y.C. Zheng, J. Hard. Mater. 159 (2008) 587.
[11] M. Sutcu, S. Akkurt, S. Okur, Ceram. Int. 35 (2009) 2571.
[12] G.K. Layden, G.W. Brindley, J. Am. Ceram. Soc. 46 (1963) 518.
[13] J.A. Dumesic, G.W. Huber, J.N. Chheda, C.J. Barrett, Stable, aqueous-phase, basic catalysts and reactions catalyzed thereby, Patent WO 2007/103858 A2, 2007.
[14] I. Sádaba, M. Ojeda, R. Mariscal, J.L.G. Fierro, M.L. Granados, Appl. Catal. B, doi:10.1016/j.apcatb.2010.11.005, (in press).
[15] M.A. Aramendia, V. Borau, C. Jimenez, A. Marinas, J.M. Marinas, J.A. Navio, J.R. Ruiz, F.J. Urbano, Colloid Surf. A 234 (2004) 17.
[16] L. Chen, J. Hu, R. Richards, ChemPhysChem 9 (2008) 1069.
[17] C.D. Wagner, L.E. Davis, M.V. Zeller, J.A. Taylor, R.H. Raymond, L.H. Gale, Surf. Interface Anal. 3 (1981) 211.
[18] D.A. Isacescu, F. Avramescu, Rev. Roum. Chim. 23 (1978) 865.
[19] D.A. Isacescu, F. Avramescu, Rev. Roum. Chim. 23 (1978) 873.
[20] B.M. Choudary, M.L. Kantam, P. Sreekanth, T. Bandopadhyay, F. Figueras, A. Tuel, J. Mol. Catal. A 142 (1999) 361.
[21] P. Afanasiev, A. Thiollier, M. Breysse, J.L. Dubois, Top. Catal. 8 (1999) 147.
[22] G.K. Chuah, Catal. Today 49 (1999) 131.
[23] R. Castro, P.J.B. Marcos, A. Lorriaux, M. Steil, L. Gengembre, P. Roussel, D. Gouvêa, Chem. Mater. 20 (2008) 3505.
[24] M. Weller, B. Damson, A. Lakki, J. Alloys Compd. 310 (2000) 47.